New Hydrophobic Treatment for the Protection of Gypsum Artifacts

Laura Bergamonti[1]*, *Edoardo* Verza[1], *Gilberto* Di Virgilio[1], *Giacomo* Muroni[2], Elena Michelini[2], *Daniele* Ferretti[2], *Pier Paolo* Lottici[3], *Claudia* Graiff[1]

[1]Dept. Chemistry, Life Sciences and Environmental Sustainability, University of Parma, 43124 Parma
[2]Dept. Engineering and Architecture, University of Parma, 43124 Parma
[3]Dept. Mathematical, Physical and Computer Sciences, University of Parma, 43124 Parma

Abstract. Gypsum has been widely used in traditional and monumental architecture in many countries of the Mediterranean area; however, due to its low water resistance and low mechanical strength, it can be subject to physical, chemical and biological degradation. To improve the preservation of gypsum-based plaster artifacts, a new hybrid inorganic-organic hydrophobic treatment is proposed in this work. This treatment is based on nanometric magnesium hydroxide ($Mg(OH)_2$) and organically modified silica (OrMoSil), a class of materials with intermediate performances between ceramic materials and polymers. The behaviour of the product was verified both as a protective on gypsum surface, as well as a consolidant added to the mixture of gypsum-based plasters. The treatment does not alter the aesthetic appearance of the surface, as verified through colorimetric analysis. As demonstrated by capillary water absorption and static contact angle measurements, the new hydrophobic protective coating proved to be very effective. Moreover, the new treatment is effective as a consolidant, leading to an improvement of the mechanical properties and to a reduction of the depth of carbonation. The new hydrophobic nanocomposite product is therefore a promising material for the protection and consolidation of gypsum monuments and artifacts of cultural interest.

1 Introduction

Gypsum-based materials have been used in architecture for centuries, both for structural purposes and for decoration. In the latter context, the Islamic tradition stands out for the creation of elaborate polychrome coverings, giving rise to the so-called Hispano-Muslim plasters [1]. Even before that, however, ancient Egyptians and Sumerians already used gypsum-based materials for their constructions [2]. The Egyptians obtained gypsum from the heating of chalk, between 100 and 170 °C, exploiting a process known as calcination, so obtaining a product that is currently known as plaster of Paris [3]. As discussed by Vitruvius and Pliny the Elder in their works, the Romans used chalk - the so-called “Opus Albarium” - as mortar and for decorative purposes. The Romans also used plaster to make casts before

* Corresponding author: laura.bergamonti@unipr.it

These proceedings are published with the support of EuLA.

sculpting marble, or as a tool for replicating Greek statues to make marble copies [4]. It is from the advent of the Renaissance, however, that plaster casts became increasingly important. Notable examples of this technique are the gypsum models and statues realized by Canova [5].

Gypsum is the fundamental component of stucco. The term stucco is derived from the Italian tradition and was widely used by Giorgio Vasari [6]. Currently, this term is used to refer to any plaster intended for decorative purposes, which could be in low or high relief, as well as to plaster walls and ceilings, especially when gypsum is used as the binder fraction. The technique was widely applied in Italy, Spain, Portugal and in the Northern Europe between the seventeenth and eighteenth centuries. Stucco has a variable composition and can be obtained following different recipes. Basically, it is a combination of plastic materials (such as gypsum and/or lime, which become solid in presence of water, after chemical transformation), fillers (such as sand, marble dust, pozzolana, and gravel), and additives that modify the physical and chemical characteristics of stucco (plasticity, setting time, adhesion, humidity resistance, mechanical strength, brilliance, etc.). These components can be either mineral or organic.

The degradation observed on gypsum plaster artifacts encompasses a wide spectrum of light defects, such as colour alteration, and more severe defects, such as the lack of cohesion of the material [1,7]. This degradation often results from a combination of hygrometric effects, structural deterioration and human factors [8]. The primary deterioration issues in gypsum-based decorations and renders are the presence of moisture, mold growth, salt efflorescence and cracking. These factors not only result in aesthetic concerns but can also compromise the integrity of the material. This kind of damage originates from the combined action of water that rises through capillary action from the ground, rainwater, as well as humidity that is naturally present in the atmosphere. Furthermore, water facilitates the development of fungi and algae on surfaces, which can in turn contribute to the desegregation and loss of material, as well as to chromatic changes of the surfaces themselves.

One of the most challenging objectives in monumental stone restoration is the synthesis of new materials for application as consolidants and/or protective agents with hydrophobic properties, in order to prevent the penetration of water [9-12]. In this research, a novel hydrophobic treatment based on nano-$Mg(OH)_2$ and organically modified siloxane (OrMoSil) is proposed as a tool to enhance the preservation of gypsum and gypsum-based plaster artifacts. OrMoSil is synthesized by the sol-gel process, consisting in the hydrolysis of the alkoxysilane to form silanol groups, followed by co-condensation between the newly formed silanol groups and the silanol groups of the organic precursor [13]. As known, organically modified siloxanes are a class of materials with intermediate performance between “pure ceramic” and “pure polymers”. The addition of the organic fraction confers toughness and flexibility to the silica network, preventing the breakdown of the gel during drying [14]. Furthermore, the introduction of aliphatic groups in the silica polymer allows the design of a material with hydrophobic properties [15]. Moreover, the addition of nanoparticles can enhance the surface hydrophobicity of a coating [16] and also avoid the cracking of the gel network during the drying phase [17]. The final product based on OrMoSil and nanoparticles of magnesium hydroxide is a clear colloidal sol. This product can be applied as a coating on the surface of gypsum-based samples, or as an additive incorporated into the mixture. The coating reduces significantly carbonation and exhibits excellent hydrophobic properties, as measured by the contact angle on the surface, and the water absorption by capillarity of the treated samples. The incorporation of the product into the mixture of the gypsum-based samples enhances instead their mechanical performances.

2 Materials and methods

2.1 Raw materials

Tetraethyl orthosilicate (TEOS, 99%), hydroxyl-terminated polydimethylsiloxane (PDMS, average Mn ~550, viscosity ~25 cSt), oxalic acid dihydrate (OxAc, 99%), sodium hydroxide (NaOH pellets, anhydrous, 98%), phenolphtalein, calcium carbonate ($CaCO_3$, 99%) and urea (CH_4N_2O, 99%) were purchased from Sigma-Aldrich. Magnesium Chloride ($MgCl_2$) and ammonium hydroxide (NH_4OH) were acquired from Merck. Gypsum and calcium hydroxide were purchased from Vigor and Unicalce, respectively. Reagents and solvents were used as received, without further purification.

2.2 Synthesis of treatment based on organically modified silica (OrMoSil) and magnesium hydroxide ($Mg(OH)_2$)

The organically modified silica (hereafter called OrMoSil) was prepared by the sol-gel method, using TEOS as inorganic precursor and PDMS as organic precursor [9]. Ethanol and de-ionized water were used as solvents, while OxAc was used as catalyst. TEOS, EtOH, H_2O and OxAc in molar ratios 1:15:15:0.00015 were vigorously stirred at room temperature for 140 min, to favor the TEOS hydrolysis; then PDMS (in TEOS/PDMS ratio 1/0.1 v/v) was slowly added to the previous solution and stirred for 90 min, to complete the condensation between the silanol groups of TEOS and the hydroxyl groups of PDMS. A portion of the final product was dried in a ventilated oven and then characterized.

The magnesium hydroxide nanoparticles were synthesized by precipitation with urea as the key reagent, to control their growth. NaOH, urea and ethanol were dissolved in water and a solution of magnesium chloride 4M was then added dropwise into the flask. The mixture was stirred at 60 °C for 1 h and the obtained suspension was allowed to precipitate for 10 h at the same temperature. The precipitate was washed with slightly alkaline water, dried in vacuum at 60 °C and a white powder was obtained.

The final product, named Mg-Hy, was prepared by mixing the OrMoSil sol with a suspension of $Mg(OH)_2$ 4 M, in volume ratio 1/1. A small amount of the Mg-Hy was dried in ventilated oven and characterized by means of X-ray powder diffraction, Raman and FTIR spectroscopies.

The compatibility and effectiveness of the hydrophobic Mg-Hy were tested both as coating, applied on gypsum surface by brush, and as consolidant, mixed with gypsum.

2.3 Preparation of gypsum samples

Two types of gypsum plaster formulations were prepared: 1) G_{Ref}, made according to an ancient recipe, mixing commercial gypsum powder with $Ca(OH)_2$ in a weight ratio of 1:1 and rabbit glue (1% of the total solid mass). The water/solid (w/s) ratio was 0.7; 2) G_{HyP}, obtained by mixing G_{Ref} with Mg-Hy in weight ratio 10 % on the total mass, with a w/s ratio 0.5.

G_{Ref} formulation was poured into 50x50x10 mm^3 silicone moulds, that were stored for 24 h at rooms conditions; subsequently, samples were demoulded and cured in a dryer. G_{Ref} samples were then coated with Mg-Hy for the chemical-physical characterization: they are named G_{HyC}.

The G_{HyP} and G_{Ref} (as control) formulations were also cast into 40x40x160 mm^3 prismatic moulds for the mechanical tests, stored for 24 h at room conditions; subsequently, samples were demoulded and cured in a dryer. In table 1 are listed the tests performed on the samples.

Table 1. Tests performed on the different types of samples. The size of the samples is indicated.

	G_{Ref}		G_{HyC}	G_{HyP}
Size (mm^3)	**50x50x10**	**40x40x160**	**50x50x10**	**40x40x160**
Water absorption	x	x	x	
Colour measurement	x		x	
Carbonation resistance	x		x	
Static Contact Angle	x		x	
Mechanical tests		x		x

2.4 Methods

2.4.1 Characterization of $Mg(OH)_2$ nanoparticles and hybrid hydrophobic (OrMoSil and Mg-Hy)

The hybrid hydrophobic formulations Mg-Hy and OrMoSil and the synthesized $Mg(OH)_2$ were characterized by means of X-ray powder diffraction (XRPD) and Raman and FTIR vibrational spectroscopies.

XRD patterns were collected on powder samples by means of a Thermo ARLX'TRA X-ray diffractometer equipped with Si–Li detector (Thermo Fisher Scientific Inc., Waltham, MA, USA). As X-Ray source the Cu-Kα radiation (40 kV and 40 mA) was used. The measurements were made at a 0.2°/min scan rate (in 2 θ) in the range 10–60° with a step size of 0.01°. Powdered silicon was used for 2θ calibration. The identification of crystalline phases was done by comparison with JCPDS (Joint Committee on Powder Diffraction Standard) cards.

Raman measurements were performed in a back-scattering geometry with a LabRAM micro-spectrometer (Jobin Yvon Horiba, Kyoto, Japan) equipped with an Olympus BX40 microscope (Olympus Corporation, Tokyo, Japan). The Raman spectra were collected, at room temperature, by a long working distance × 50 microscope objective lens, using the 632.8 nm line of a 15 mW He-Ne laser. The data were elaborated by LabSpec 5.78.24 software (Jobin Yvon Horiba, Kyoto, Japan) and as reference the Ruff database was used. The FTIR spectra were acquired in the range 4000-400 cm^{-1} with a spectral resolution of 4 cm^{-1} and penetration depth ≈ 2 μm, using the Thermo-Nicolet Nexus spectrometer equipped with Thermo Smart Orbit ATR diamond accessory, in ATR mode: 16 scans for each spectrum were collected.

2.4.2 Characterization of gypsum-based plaster coated with hydrophobic Mg-Hy treatment (G_{HyC})

Morphological investigations and elemental analysis before and after the treatments were performed by means of a SEM-EDS system: a scanning electron microscope Jeol 6400 (Jeol Ltd.; Tokyo, Japan) equipped with an Oxford Instruments (Abingdon-on-Thames, UK) Analytical Link Si(Li) Energy Dispersive System Detector, with INCA V7.2 software.

The chromatic changes in the stone surface's appearance due to the Mg-Hy coating were assessed according to UNI EN 15886:2010 [18] by colorimetric measurements using a Spectrodens colorimeter (Techkon GmbH, Königstein, Germany). The measurements were collected on nine small zones and the results were averaged on three samples. The total color difference (ΔE*) due to the coating was measured as:

$$\Delta E^* = \sqrt{\Delta L^{*2} + \Delta a^{*2} + \Delta b^{*2}} \quad (1)$$

where ΔL* is the change in lightness, Δa* and Δb* are the changes of the colorimetric coordinates a* (opposing colours red/green) and b* (opposing colours yellow/blue) in the CIELAB space.

To evaluate the hydrophobic properties of the Mg-Hy coating, static contact angle measurements were taken by the OCA25 device (DataPhysics Instruments, Filderstadt, Germany), using the sessile drop method, with 5 μL drops applied via a needle to the stone surface before and after treatment, according to UNI 11207:2007 [19].

The water absorption by capillarity was measured on three treated samples, according to UNI EN 15801:2010 [20]. The dried samples were placed on 1 cm thick Whatman multilayer paper, saturated with deionized water. Samples were weighed at times t_i =10 min, 20 min, 30 min, 60 min, 2 h, 4 h and 6 h, and at subsequent 24 h intervals until the difference between two consecutive weighing was <1% of the initial weight of the samples. The amount of absorbed water per unit area Q_i (kg/m^2) was determined by:

$$Q_i = \frac{M_i - M_0}{A} \quad (2)$$

where M_i e M_o are the sample masses (kg) at time t_i and at the initial time, respectively, and A is the area of the specimen in m^2. The Q_i values were reported as a function of the square root of time ($t_i^{1/2}$), according to a well-known capillarity absorption model [21], which gives at short times a linear relationship between the adsorbed water and the square root of time. The value of the capillary water absorption coefficient AC (kg/(m^{2}s$^{1/2}$) was obtained as the slope of the linear fit to the first part (up to 60 min) of the capillarity graph (Q_i).

To evaluate the effectiveness of hydrophobic treatments, a carbonation resistance test was carried out under both artificial and natural conditions. For the tests in artificial conditions, coated and uncoated specimens were placed inside a carbonation chamber at 20 °C, RH 60% and 5% CO_2 and left for 12 months. CO_2 was produced by the reaction between hydrochloric acid and carbonate rocks in a Kipp apparatus, and subsequently introduced inside the chamber. The reaction developed is:

$$CaCO_3 + 2HCl \rightarrow CaCl_2 + CO_2\uparrow + H_2O. \quad (3)$$

For the tests in natural conditions, the samples were exposed outdoors, close to a road and a car park, and left for 6 months. The weather conditions are summarized in table 2.

The measurement of the resistance to carbonation of the gypsum specimens coated with the hydrophobic treatment was carried out using a colorimetric method with phenolphthalein solution (1% in ethanol), a colourless compound in a neutral environment. The application of phenolphthalein to the surface of the specimens resulted in a colour change depending on the change in pH (turning to lilac in an alkaline environment pH ≥ 8.3).

Table 2. Average temperature, total rain and relative humidity (RH %).

Weather parameters	March	April	May	June	July	August
Temperature (°C)	12.3	14.2	18.9	24.9	28.1 (max 38.8)	27.5 (max 40.4)
Rain (mm)	5.1	10.6	150.2	55.6	27	31.6
RH (%)	64	61.5	70.8	59.3	55	51.1

2.4.3 Mechanical characterization on gypsum-based plaster embedded with hydrophobic product Mg-Hy (G_{HyP})

To assess the effectiveness of Mg-Hy product as a consolidant, mechanical tests were performed on the G_{HyP} admixture and on the reference admixture G_{Ref}, serving as control. Obviously, the simple application of the hydrophobic treatment on the external surface of the specimens does not to alter the mechanical performance of the material.
The determination of dynamic elastic modulus (through the determination of ultrasonic pulse velocity) was carried out according to EN 12504-4 [22], on three 40 x 40 x 160 mm^3 prismatic samples, which were preliminarily oven-dried at 60 °C. The dynamic elastic modulus was determined through the relation:

$$E_d = v^2 \rho [(1+\nu) (1- 2\nu)]/(1- \nu) \quad (4)$$

where v is the ultrasonic pulse velocity, ρ is the specific mass at the hardened state, and ν is the Poisson coefficient, assumed equal to 0.22.
Flexural and compressive strengths were determined according to EN 1015-11 [23]. Flexural tests were carried out on the same samples under a three-point bending scheme, by using an MTS 2/M Universal testing machine. After failure, the two remaining halves of each prism were tested in compression, by using an INSTRON 5882 Universal machine.

3 Results and discussion

3.1 Characterization of $Mg(OH)_2$ nanoparticles and hybrid hydrophobic (OrMoSil and Mg-Hy)

Figure 1a reports the XRPD pattern of the Mg-Hy product compared to those of OrMoSil and $Mg(OH)_2$.

The XRPD pattern of magnesium hydroxide nanoparticles corresponds to a hexagonal structure (in accordance with the JCPDS 7-0239 standard card) [24-25] and indicates a lamellar structure with layers in [001] direction. The nanoparticles size is about 15 nm, as estimated by Scherrer equation, based on Full Width at Half-Maximum (FWHM). FWHM was obtained by a deconvolution procedure using a pseudo-Voigt function (Figure 1b). In the Scherrer equation (eq 5), D is the particle size, K is a dimensionless shape factor, λ is the X-ray wavelength, B is the line broadening at half the maximum intensity (FWHM), in radians, and θ is the Bragg angle. In figure 1a asterisks indicate features due to residues of NaCl, formed during the preparation.

$$D = \frac{K\lambda}{\beta \cos\theta} \approx 15.4\, nm \quad (5)$$

The diffraction pattern of the Mg-Hy is dominated by the $Mg(OH)_2$ pattern, with a small background due to the amorphous component. Amorphous features introduced by OrMoSil are indicated with arrows.

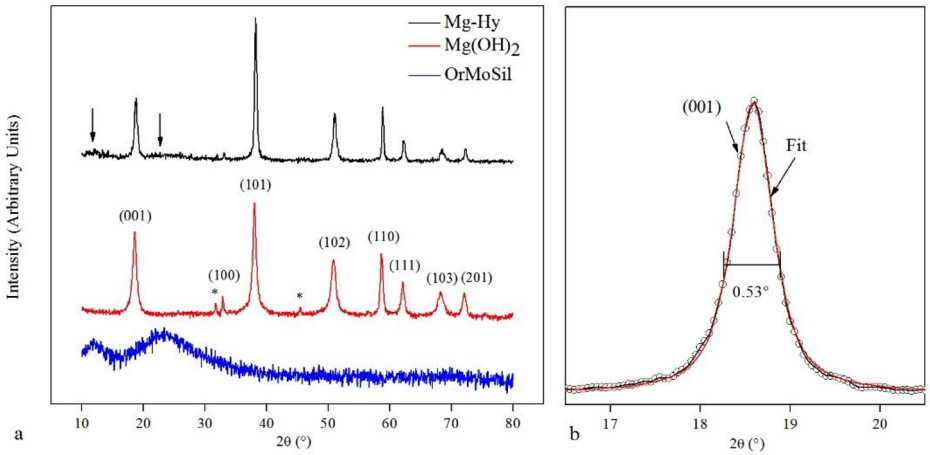

Fig. 1. XRPD pattern of Mg-Hy compared to $Mg(OH)_2$ and OrMoSil (a); deconvolution procedure using a pseudo-Voigt function (b).

The Raman and FTIR spectra are reported in Figures 2a and 2b, respectively. In the Raman spectrum of the Mg $(OH)_2$ samples, the identifying peaks at 445 cm^{-1} and at 280 cm^{-1} are evident [26]. The Raman spectrum of OrMoSil is dominated by the characteristic features of PDMS: Si-O-Si symmetric stretching (495 cm^{-1}), CH_3 rocking vibration (shoulder at 677 cm^{-1}), C-Si-C symmetric stretching (713 cm^{-1}), Si-C asymmetric stretching vibration (795 cm^{-1}), CH_3 symmetric rocking (865 cm^{-1}), CH_3 symmetric bending (1265 cm^{-1}) and CH_3 asymmetric bending (1409 cm^{-1}) [27-28]. The vibrations of siloxane network yield to low intensity Raman peaks, however, the weak peak at 990 cm^{-1} due to silanol terminal groups, is observable. In the Mg-Hy product, the peaks of magnesium hydroxide and OrMoSil are visible.

The FTIR spectrum of magnesium hydroxide, in agreement with literature [29], shows a sharp and intense –OH stretching vibration peak at 3698 cm^{-1} and two medium-weak bands at 1635 and 1406 cm^{-1} attributed to the –OH bending vibration and Mg–O stretching vibration, respectively.

The main bands in the FTIR spectrum of OrMoSil are associated with the Si-O-Si network formed by TEOS condensation and to Si-C bonds from PDMS [28,30]. For the TEOS the asymmetric and symmetric Si–O–Si stretching vibrations are observed at 1084 cm^{-1} and at 1018 cm^{-1}, respectively. The typical bands of PDMS are observed at 2960 cm^{-1} for the CH_3 stretching vibration and at 1260 cm^{-1} and at 792 cm^{-1} for the asymmetric and symmetric Si–CH_3 stretching vibrations, respectively [31]. In the FTIR spectrum of the final product Mg-Hy the features of both $Mg(OH)_2$ and OrMoSil are clearly observable.

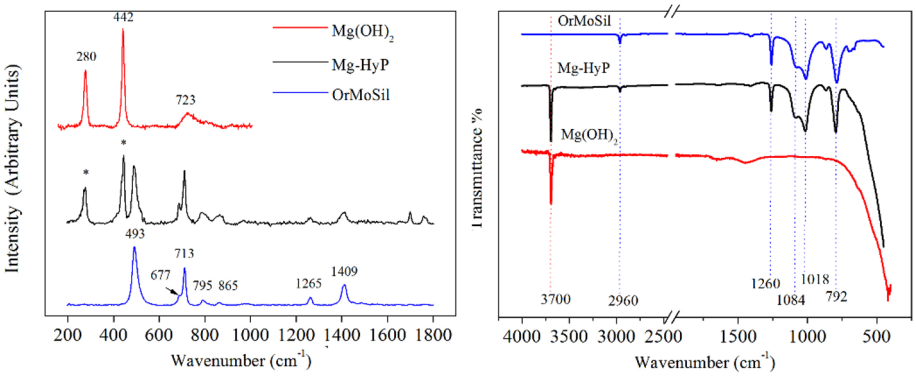

Fig. 2. (a) Raman and (b) FTIR spectra of Mg-Hy compared to those of OrMoSil and $Mg(OH)_2$.

3.2 Characterization of gypsum-based plaster coated with hydrophobic Mg-Hy treatment (G_{HyC})

The morphology of G_{Ref} and gypsum-based G_{HyC} samples was investigated through SEM analysis: images are reported in Figures 3a, 3b. The surface of the samples has a homogeneous microstructure characterized by a micro-porosity with pores of ≈ 30-50 µm. Figure 3c shows the Si and Mg elemental maps and the EDS spectrum, acquired on the area within the yellow line of Figure 3b. The elemental maps highlight a homogeneous distribution of Si over the entire surface, while Mg shows small aggregates of nanoparticles.

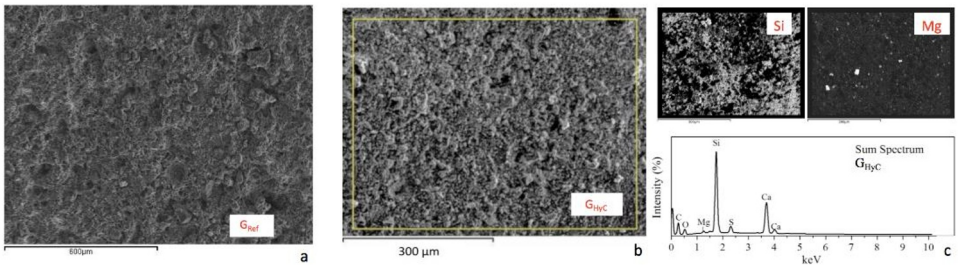

Fig. 3. SEM images of G_{Ref} (a) and G_{HyC} (b) with elemental maps of Si and Mg (c).

To test the harmlessness of the coating treatment, colorimetric analysis was performed, and the change of the stone surface appearance was evaluated. The color difference (ΔE*) due to coating application with respect to the uncoated G_{Ref} was measured in the CIELab colorimetric space [18]. The results show that the coating does not alter the aesthetic appearance of the samples. The measured value of ΔE* is 1.2±0.3, well lower than the threshold of ΔE* ≈ 3, below which the eye is unable to perceive the color difference.

The most important result for the G_{HyC} samples is shown in Figure 4: The (Mg-Hy) coating gives super-hydrophobic properties to the gypsum surface, since the contact angle measured is nearly 150°. Due to the immediate absorption of the water drop, obviously the contact angle on the pure gypsum surface cannot be measured.

The efficiency of the coating in reducing the water absorption by capillarity was evaluated by comparative measurements on G_{Ref} and G_{HyC} samples. The amount of absorbed water Q_i is reported as a function of the square root of time in Figure 5. The results emphasize that the hydrophobic treatment induces a significant decrease of the water absorption, by almost 50%.

The absorption coefficient AC_{60}, obtained as the slope of the linear fit to the first part (up to 60 min) of the capillarity graph (Q_i), is significantly lower in the coated sample.

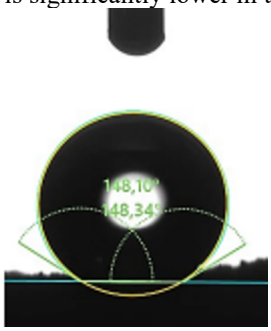

Fig. 4. Static contact angle measured on G_{HyC} sample.

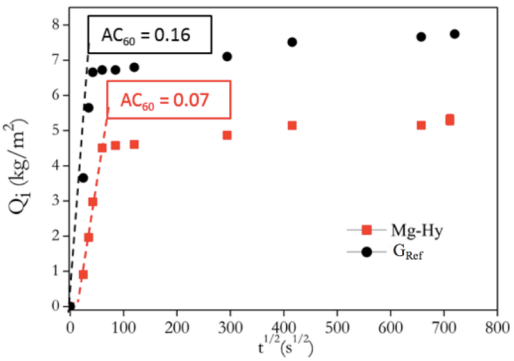

Fig. 5. Absorbed water Q_i reported as a function of the square root of time.

The phenomenon of carbonation is dangerous because the lowering of the pH can trigger corrosive phenomena in iron elements often used as frame in gypsum artifacts. For the evaluation of the carbonation, the surfaces of the treated and untreated samples, just broken, were sprayed with a phenolphthalein (1%) alcoholic solution, colourless in neutral/acid environment turning to lilac in an alkaline environment.

As evident in Figure 6 the carbonation in the G_{HyC} is limited to a depth to a few mm from the surface, while in uncoated G_{Ref} sample it is present in the entire section. The hydrophobic Mg-Hy coating hinders the CO_2 diffusion inside the stone, keeping the pH at values higher than 8.3.

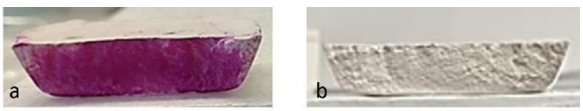

Fig. 6. Carbonation test on (a) G_{HyC} and (b) G_{Ref}.

3.3 Characterization of gypsum-based plaster embedded with hydrophobic product Mg-Hy (G_{HyP})

The efficiency of the new hydrophobic Mg-Hy product as a consolidant was tested on G_{HyP} samples. The morphology and the elemental distribution of Mg-Hy inside the G_{HyP} samples was performed by means of SEM-EDS analyses (Figure 7). The plaster appears uniform and

smoothed. This effect is more evident in the SEM image of the reference plaster sample as reported in Figure 3a.

EDS elementary maps were acquired on the cross section of samples: Mg and Si are homogeneously distributed inside the G_{HyP} plaster.

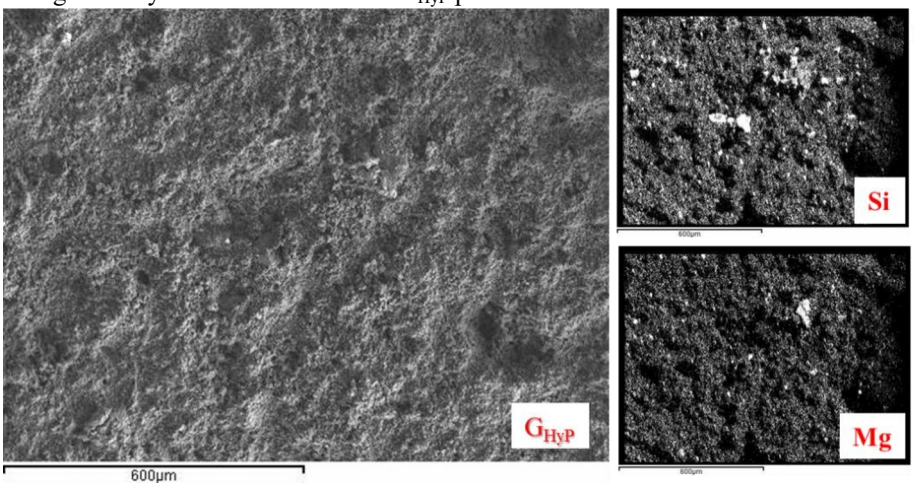

Fig. 7. SEM image of G_{HyP} and Si and Mg maps collected on the entire area.

Figure 8 shows the impact of the novel hydrophobic treatment on the mechanical properties of gypsum-based material (G_{HyP}) after 28 days of curing. The hydrophobic treatment induces an increase of the dynamic elastic modulus E_d of nearly 35% with respect to the G_{Ref} (Figure 8a).

The incorporation of the Mg-Hy product into G_{Ref} causes an increase of the flexural and compressive strength by 59% and 72%, respectively, (Figure 8b), so attesting its effectiveness as a consolidant.

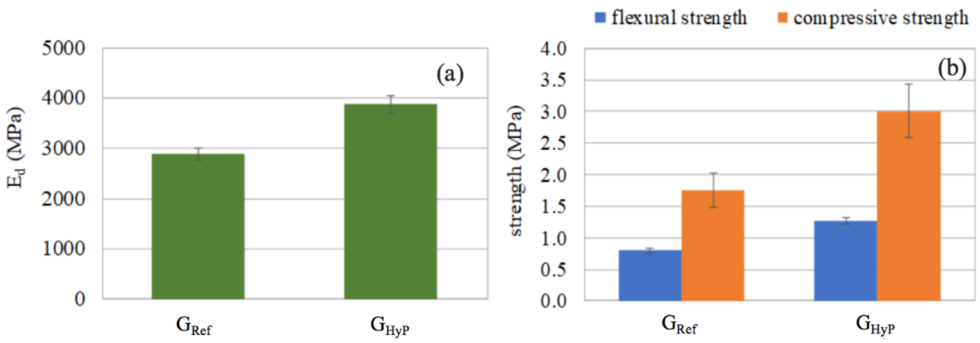

Fig. 8. (a) Dynamic elastic modulus and (b) flexural and compressive strengths in G_{Ref} and G_{HyP}.

4 Conclusions

The performance of the new hydrophobic formulation based on $Mg(OH)_2$ nanoparticles and OrMoSil, was verified both as a protective on gypsum surface, as well as a consolidant added to the mixture of gypsum-based plasters. The proposed coating results to be an effective hydrophobic protective: the water absorption by capillarity is reduced of about 50% and the static contact angle is nearly 150°. The aesthetic appearance of the surface is not altered by the coating. Moreover, it is effective to reduce the depth of carbonation. Further studies are

underway to investigate the durability of the treatment and the effect of reducing water vapour permeability: the latter represents the greatest criticality when the hydrophobic protective is used on porous materials, such as gypsum plaster.
The new hydrophobic formulation added to the gypsum-based plaster improves the mechanical properties leading to an increase of the flexural and compressive strength by 59% and 72% respectively.

The new hybrid inorganic-organic hydrophobic treatment acts as a promising material for the protection and consolidation of gypsum monuments and artifacts of cultural interest.

Acknowledgements: This research was supported by NextGenerationEU—Italian Ministry of University and Research, National Recovery and Resilience Plan (NRRP); Project "Ecosystem for Sustainable Transition in Emilia-Romagna (Ecosister)"; Project code ECS00000033. This work has benefited from the equipment and framework of the COMP-R Initiative, funded by the "Departments of Excellence" program of the Italian Ministry for University and Research (MUR, 2023–2027).

References

1. A.G. Bueno, V.J.M. Flórez, The Nasrid plasterwork at "qubba Dar al-Manjara l-kubra" in Granada: characterisation of materials and techniques, J. Cult. Herit. **5**, 75–89 (2004).
2. L. Rehhof, P. Akkermans, E. Leonardsen, I. Thuesen, Plasters: gypsum or calcite? A preliminary case study of Syrian plasters, Paléorient. 79–87 (1990).
3. J. A. Harrell, Amarna gypsite: A new source of gypsum for ancient Egypt. Journal of Archaeological Science: Reports. **11**, 536-545 (2017).
4. R. Frederiksen, E. Marchand, Plaster casts: making, collecting and displaying from classical antiquity to the present, (Walter de Gruyter, 2010).
5. J. Myssok, C.R. Marshall, The Gipsoteca of Possagno. From Artist's Studio to Museum, (Sculpt. Museum. 2011).
6. G. Vasari, Opere di Giorgio Vasari (Tipografia de' fratelli Ubicini, 1840).
7. M. Anzani, M. Berzioli, M. Cagna, E. Campani, A. Casoli, P. Cremonesi, M. Fratelli, A. Rabbolini, D. Riggiardi, Gel rigidi di agar per il trattamento di pulitura di manufatti in gesso (Use of rigid agar gels for cleaning plaster objects), (QUADERNO N.6/CESMAR7, 2008).
8. H. Cotrim, M. do Rosário Veiga, J. de Brito, Freixo palace: Rehabilitation of decorative gypsum plasters, Constr. Build. Mater. **22**, 41–49 (2008).
9. L. Bergamonti, M. Potenza, F. Scigliuzzo, S. Meli, A. Casoli, P. P. Lottici, & C. Graiff, Hydrophobic and Photocatalytic Treatment for the Conservation of Painted Lecce stone in Outdoor Conditions: A New Cleaning Approach. Applied Sciences. **14**, 1261 (2024).
10. A. P. Kanth, & A. K. Soni, Application of nanocomposites for conservation of materials of cultural heritage. Journal of Cultural Heritage. **59**, 120-130 (2023)
11. C. Kapridaki, L. Pinho, M. J. Mosquera, P. Maravelaki-Kalaitzaki, Producing photoactive, transparent and hydrophobic SiO_2-crystalline TiO_2 nanocomposites at ambient conditions with application as self-cleaning coatings. Appl. Catal. B. **156**, 416–427 (2014).
12. M. J. Mosquera, D. M. De Los Santos, T. Rivas. Surfactant-synthesized ormosils with application to stone restoration. Langmuir. **26**, 6737–6745 (2010).
13. P. Lacan, C. Guizard, L. Cot, Chemical and rheological investigations of the sol-gel transition in organically-modified siloxanes, J. Sol-Gel Sci. Technol. **4**, 151–162 (1995).

14. D. Li, F. Xu, Z. Liu, J. Zhu, Q. Zhang, L. Shao. The effect of adding PDMS-OH and silica nanoparticles on sol–gel properties and effectiveness in stone protection. Appl. Surf. Sci., **266**, 368–374 (2013).
15. I. Karapanagiotis, A. Pavlou, P. N. Manoudis, & K. E. Aifantis. Water repellent ORMOSIL films for the protection of stone and other materials. Materials Letters. **131**, 276-279 (2014).
16. P.N. Manoudis, A. Tsakalof, I. Karapanagiotis, I. Zuburtikudis, C. Panayiotou. Surface & Coatings Technology, **203**, p. 1322 (2009).
17. E. K. Kim, J. Won, J. Do, S.D. Kim, Y.S. Kang. Journal of Cultural Heritage, **10**, (2010).
18. EN 15886:2010, Conservation of cultural property - Test methods - Colour measurement of surfaces, 2010.
19. UNI 11207:2007, Cultural heritage - Natural and artificial stones - Determination of static contact angle on laboratory specimens, 2007.
20. UNI EN 15801:2010, Conservation of cultural property - Test methods - Determination of water absorption by capillarity, 2010.
21. E.W. Washburn, The Dynamics of Capillary Flow. Phys. Rev. **17**, 273 (1921).
22. EN 12504-4:2021, Testing concrete in structures - Part 4: Determination of ultrasonic pulse velocity, 2021.
23. EN 1015-11:2020-01, Methods of test for mortar for masonry - Part 11: Determination of flexural and compressive strength of hardened mortar; German version EN 1015-11:2019, 2020.
24. K.M. Saoud, S. Saeed, R.M. Al-Soubaihi, M.F. Bertino, Microwave assisted preparation of magnesium hydroxide nano-sheets, Am. J. Nanomater. **2**, 21–25 (2014).
25. W. Jiang, X. Hua, Q. Han, X. Yang, L. Lu, X. Wang, Preparation of lamellar magnesium hydroxide nanoparticles via precipitation method, Powder Technol. 191, 227–230 (2009).
26. F. Pascale, S. Tosoni, C. Zicovich-Wilson, P. Ugliengo, R. Orlando, R. Dovesi, Vibrational spectrum of brucite, Mg $(OH)_2$: a periodic ab initio quantum mechanical calculation including OH anharmonicity, Chem. Phys. Lett. **396**, 308–315 (2004).
27. S.C. Bae, H. Lee, Z. Lin, S. Granick, Chemical imaging in a surface forces apparatus: confocal Raman spectroscopy of confined poly (dimethylsiloxane), Langmuir. **21**, 5685–5688 (2005).
28. A. Tamayo, J. Rubio, Structure modification by solvent addition into TEOS/PDMS hybrid materials, J. Non. Cryst. Solids. **356**, 1742–1748 (2010).
29. H. Dong, Z. Du, Y. Zhao, D. Zhou, Preparation of surface modified nano-Mg $(OH)_2$ via precipitation method, Powder Technol. **198** (2010) 325–329.
30. Kapridaki, & P. Maravelaki-Kalaitzaki, TiO_2–SiO_2–PDMS nano-composite hydrophobic coating with self-cleaning properties for marble protection, Prog. Org. **76** (2-3), 400-410 (2013).
31. R. Basile, L. Bergamonti, F. Fernandez, C. Graiff, A. Haghighi, C. Isca, P. P. Lottici, B. Pizzo, & G. Predieri, Bio-inspired consolidants derived from crystalline nanocellulose for decayed wood, Carbohydrate polymers, **202**, 164-171 (2018).